DFT Investigation of CH4 and H2O Adsorption on Pd (111), Ni (111), Pt (111), and Ir(111) Surfaces

Abdulrauf Onimisi Ibrahim[1,2]*, Baba Jibril El-Yakubu[2]

[1] *Department of Chemical Engineering,*
   Universiti Malaya, Kuala Lumpur, MALAYSIA

[2] *Department of Chemical Engineering,*
   Ahmadu Bello University, Zaria, NIGERIA

*Corresponding Author: s2003719@siswa.um.edu.my
DOI: https://doi.org/10.30880/jst.2023.15.02.008

Article Info

Abstract

Using density functional theory (DFT) calculations, the surface Gibbs free energy of methane and water adsorption on Pt(111), Ir(111), Ni(111), and Pd(111) surfaces was investigated. DFT computations were employed to investigate the adsorption of methane and water molecules on unit cells with varying coverage levels of 0.11, 0.25, 0.50, and 1.00 monolayers and the aggregation of H_2O over clean transition metal surfaces. The adsorption configuration was assessed to experimental findings to evaluate our computational approaches' accuracy and reliability. A thermodynamic diagram was constructed for exploring the adsorption of CH4 and H2O on metal surfaces. The order of the methane adsorption energies on different metal surfaces is as follows: Pd(111) > Pt(111) > Ni(111) > Ir(111). A more significant number of H_2O molecules on the transition metal surfaces reduces the contact between the metal surfaces and water molecules during water aggregation. The thermodynamic stability of water and methane adsorption coverage was found to be best on the Pt(111) surface.

1. Introduction

The commercial significance of the catalytic breakdown of CH_4 on metallic surfaces is remarkable [1]. CH_4 is a primary constituent of natural gas and plays a remarkable role in hydrogen generation. The primary methods utilised in the production of hydrogen include methane steam reforming (SRM) [$CH_4 + H_2O \rightarrow + 3H_2 + CO$] [2], partial oxidation of methane [$CH_4 + \frac{1}{2}O_2 \rightarrow 2H_2 + CO$] [3], and methane dry reforming [$CO_2 + CH_4 \rightarrow CO + 2H_2$] [4]. The SRM is the process by which CH_4 and H_2O react over a nickel catalyst, accounting for nearly 98% world's supply of hydrogen gas[5]. To get a high conversion of methane, it is necessary to employ a reactor operating at elevated temperatures ranging from 700°C to 1,000°C [6]. This is due to the fact that the process involving methane is entirely endothermic. The utilisation of optimal catalysts is imperative within the industrial sector to enhance the efficiency of methane steam reforming. Furthermore, the comprehension of catalytic reactions can be achieved through the application of quantum chemistry principles [7].

   Water and methane adsorption on transition metal surfaces have been the attention of numerous studies. Many articles have confirmed that the single water molecule favours adsorbing at the atop site on metal surfaces [8-10]. Pache et al. [11] conducted a study to examine the water adsorption process on a clean Ni(111) surface, spanning from low to saturation coverage. The researchers observed a desorption peak within the temperature range of 438-443°C. This peak can be attributed to water molecules in the 1st monolayer and the hydrogen bonding interactions among these water molecules. Additionally, the adsorption energy of a single water

molecule was determined to be 0.44 eV. Chen et al. [12] examined the physisorption of CH_4 on Pt(111) through reflection absorption infrared spectroscopy. The researchers discovered that the desorption energy of CH_4 on the Pt(111) surface was measured to be 18.3 kJ/mol at a surface temperature of 305 °C.

The application of DFT inside a thermodynamic model allows for predicting the preferred coverages on the surface of a catalyst, considering the influence of intensive state variables. In this work, we utilised periodic DFT calculations to investigate the impact of H_2O and CH_4 adsorption on the surfaces of Pt(111), Ni(111), Ir(111), and Pd(111). The calculations were performed using gradient-corrected (PW91) functionals. Thermodynamic phase diagrams employ surface Gibbs free energies (SGF) to determine the optimal adsorbate coverage on a catalyst surface, considering gas phase temperature and pressure variations.

2. Materials and Methods

2.1 Energy Calculations

Periodic DFT calculations were executed with Dmol³ of Materials Studio 8.0 [13] to analyse geometries and electronic energies at 0 K. The correlation and exchange functional were defined by generalised gradient approximation (GGA) using PW91 functional [14]in conjunction with a doubled numerical basis set plus polarisation [15]. Brillouin-zone integrations were carried out using 4×4×1, 5×5×1, 10×5×1 and 10×10×1 k-point grid for p(3×3), p(2×2), p(1×2) and p(1×1)surface, respectively. A value of 0.005 Ha was adapted for thermal smearing to obtain accurate electronic convergence. Conditions for convergence comprised a lower limit of 1.0× 10⁻⁵ Ha for energy, $5.0 \times 10^{-3} Å^{-1}$ for maximum displacement and $2.0 \times 10^{-3} \frac{Ha}{Å}$ for maximum force, and with self-consistent field convergence of 1.0×10^{-6} Ha. The lattice constants of Ni, Pt, Pd, and Ir were determined to be 3.53550 Å, 3.98950 Å, 3.96340 Å, and 3.8926 Å, respectively. These values closely matched the experimental results of 3.52 Å [16], 3.916 Å [17], 3.89 Å [18] and 3.84 Å [17] respectively.

The metal (111) surfaces were simulated using a four-layered slab, with only the top two layers relaxed while the bulk optimal structure was imposed on the other levels. The unit cell employed for the adsorption of methane and water is reproduced in all three dimensions, resulting in an endless surface with a vacuum thickness of 15 Å. Two methodologies were employed to examine the consequences of coverage. Initially, the unit cell size is manipulated while maintaining constant adsorbates. Secondly, by increasing the quantity of adsorbates within the unit cell. The initial methodology was employed to investigate the impact of methane coverage. The investigation involved the examination of methane at various coverages by the process of adsorbing a single methane molecule on unit cells with dimensions of (3×3), (2×2), (2×1), and (1×1). The selection of several surface sizes, namely p(3×3), p(2×2), p(1×2), and p(1×1), was made to accurately reproduce the distinct coverage levels of 0.11, 0.25, 0.50, and 1.00 monolayer, respectively. Figure 1 depicts the several adsorption sites on the metal (111) surface, including atop, bridge, fcc, and hcp. The determination of adsorption energy involved calculating the energy released per methane/water molecule adsorbed on the clean surface, as described by equation 1.

$$E_{ads} = E_{methane/M} - (E_M + E_{methane}) \tag{1}$$
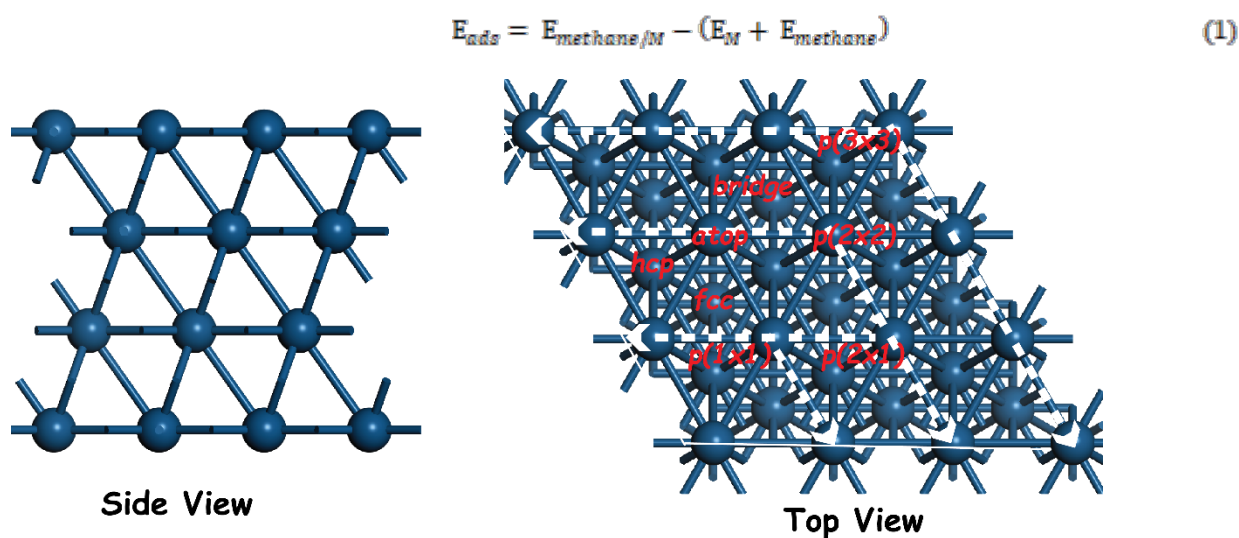
Fig. 1 *Side and top views of Ir(111) surface showing coverage of 0.11 (3x3), 0.25 (2x2), 0.50 (2x1) and 1.00 (1x1) monolayer*

The variable $E_{methane/M}$ is the slab energy of the metal surface with methane molecule adsorbed on it. E_M is the slab energy of the metal surface in the absence of the adsorbed molecules, and $E_{methane}$ is the electronic

energy of methane. This implies that the more negative E_{ads}, the stronger the interactions between the metal surface and the adsorbed species [8].

The activation energy of the reactions was determined by calculating the transition states (TS) employing linear synchronous transit and quadratic synchronous transit techniques. For the reaction, CD → C + D on X(111) catalyst, activation energy (E_A) and reaction energy (ΔE) were determined using equations 2 and 3.

$$E_A = E_{TS/X} - E_{(C+D)/X} \tag{2}$$

$$\Delta E = E_{(C+D)/X} - E_{CD/X} \tag{3}$$

The slab energy of TS is denoted by $E_{TS/X}$, the slab energy of the catalyst surface with adsorbed C and D species is denoted by $E_{(C+D)/X}$, and the slab energy of the catalyst surface with adsorbed CD species is denoted by $E_{CD/X}$.

2.2 Aggregation of H_2O on Metal Surface

For H_2O aggregation on the metal (111) surface with a (2x2) unit cell, the formation energy ($E_{formation}$) of $(H_2O)_n$ cluster on M(111) surface comprises two types of interactions; one is the interaction between the metal surface and $(H_2O)_n$ cluster; the other is within the adsorbed $(H_2O)_n$ molecules. The formation energy ($E_{formation}$) is expressed in equation (4):

$$E_{formation} = \frac{\left[E_{(H_2O)_n/M} - \left(E_M + nE_{H_2O} \right) \right]}{n} \tag{4}$$

Where E_M is slab energy of clean metal surface, $E_{H_2O_n/M}$ is slab energy for the metal surface with the adsorbed $(H_2O)_n$ cluster, n is number of H_2O molecule in $(H_2O)_n$ cluster, and E_{H_2O} is energy of H_2O molecule. The following methods are used to calculate the adsorption energy (E_{ads}^c) and hydrogen-bond interaction (E_H) of $(H_2O)_n$ system:

$$E_H = \frac{\left[nE_{(H_2O)_n} - nE_{H_2O} \right]}{n} \tag{5}$$

$$E_{ads}^c = E_{form} - E_H \tag{6}$$

Where $E_{(H_2O)_n}$ is $(H_2O)_n$ cluster single point energy.

2.3 Thermodynamic Calculations

The catalytic methane steam reforming reaction typically occurs at high temperatures between 650°C to 900°C [19]. For these conditions, density functional theory can yield entropies of elementary reaction steps using statistical thermodynamics and calculated electronic energy. The SGF energy (Γ) was used to assess the most reliable surface coverage, which is a function of the gas phase condition. Γ was determined from the Gibbs energy with vibrational frequencies contribution is calculated as shown in equation 7.

$$\Gamma(T, p_i) = \frac{G_{ads}(T) - n_M G_{bulk}(T) - \sum_i n_i G_{m,gas,i}(T, p_i)}{2 \times SA} \tag{7}$$

With G_{bulk} and G_{ads} is the Gibbs free energy of the bulk metal atom and the adsorbate coverage, respectively. SA is the unit cell surface area. n_i and n_M represent the total number of adsorbed molecules and the total number of metal atoms in the unit cell.

3. Results and Discussion

3.1 CH_4 Adsorption on Metal Surface at Different Coverage

Multiple positioning of the CH_4 molecule were investigated at all adsorption sites on the transition metal (111) surface, as depicted in Figure 1. Table 1 presents a summary of the height of methane from the metal surface (h_{M-C}), the bond length between hydrogen atoms and carbon atom (d_{C-H}), and the adsorption energies (E_{ads}) for various coverage levels of 1.00, 0.50, 0.25, and 0.11 monolayer (ML).

Table 1 - Methane adsorption on metal (111) surface

| Metal Surface	Adsorption Site	0.11 ML			0.25 ML			0.50 ML			1.00 ML		
		h_{M-C} (Å)	d_{C-H} (Å)	E_{ads} (kJ/mol)	h_{M-C} (Å)	d_{C-H} (Å)	E_{ads} (kJ/mol)	h_{M-C} (Å)	d_{C-H} (Å)	E_{ads} (kJ/mol)	h_{M-C} (Å)	d_{C-H} (Å)	E_{ads} (kJ/mol)
Pt(111)	atop	3.58	1.106	**-10.38**	3.56	1.105	**-10.99**	3.61	1.102	54.81	3.69	1.094	148.90
	bridge	3.86	1.099	-9.07	3.82	1.100	-9.93	3.82	1.098	55.91	3.84	1.092	149.32
	fcc	3.81	1.099	-8.76	3.85	1.099	-9.82	3.83	1.098	56.00	3.82	1.092	149.71
	hcp	3.75	1.100	-8.60	3.79	1.100	-9.68	3.82	1.098	56.04	3.81	1.091	149.76
Pd(111)	atop	3.43	1.106	**-12.28**	3.56	1.104	**-13.16**	3.59	1.094	38.26	3.47	1.096	157.45
	bridge	3.51	1.102	-10.37	3.54	1.102	-11.64	3.62	1.093	39.09	3.69	1.094	158.00
	fcc	3.50	1.102	-10.38	3.54	1.102	-11.16	3.62	1.093	62.10	3.63	1.094	158.45
	hcp	3.50	1.102	-10.43	3.57	1.101	-11.36	3.60	1.100	62.07	3.68	1.093	158.44
Ir(111)	atop	3.80	1.101	**-10.08**	3.95	1.099	**-11.05**	3.91	1.091	48.22	3.91	1.091	184.44
	bridge	4.12	1.097	-9.18	3.90	1.098	-9.88	4.20	1.095	71.68	3.90	1.089	185.02
	fcc	4.24	1.097	-9.07	3.89	1.098	-9.45	4.22	1.095	71.69	4.19	1.089	185.02
	hcp	4.20	1.097	-9.15	4.01	1.097	-10.13	4.22	1.096	71.77	3.91	1.089	185.03
Ni(111)	atop	3.91	1.098	**-10.33**	4.13	1.098	**-12.51**	3.89	1.088	115.77	3.72	1.092	382.62
	bridge	3.95	1.098	-10.18	4.08	1.098	-12.13	3.62	1.090	116.52	3.72	1.093	382.84
	fcc	3.97	1.098	-10.02	4.04	1.098	-12.09	3.59	1.090	116.44	3.74	1.092	382.88
	hcp	4.02	1.098	-10.02	3.81	1.100	-11.52	3.80	1.087	116.22	3.75	1.092	382.87

The favoured adsorption site for methane is the atop site on all metal surfaces, consistent with findings from earlier studies [20, 21]. At surface coverages of 0.50 and 1.00 monolayer on the metal surfaces, the adsorption energy of CH_4 exhibited a positive value, indicating that the adsorption process was thermodynamically unstable. The adsorption energies of CH_4 on the Pt(111) surface were found to be -10.99 kJ/mol and -10.38 kJ/mol for coverages of 0.25 and 0.11 ML, respectively, indicating their high stability. This finding is consistent with the previous research conducted by Gautier et al. [22] (-9.7 kJ/mol). The favoured adsorption site for methane on Pd(111) is the atop site, exhibiting adsorption energies of -12.28 kJ/mol and -13.16 kJ/mol at coverages of 0.25 and 0.11 monolayer, respectively. These values closely align with the experimental findings of -17.02 kJ/mol [23]. The preferred adsorption site for methane on Ni(111) is the atop site, exhibiting an adsorption energy of -10.33 kJ/mol 0.11 monolayer, which is in agreement with the experimental findings (Ni in carbon nanotube) [24] having an adsorption energy of -8.51 kJ/mol. According to the data presented in Table 1, it can be observed that methane exhibits the most pronounced interactions with the Pd(111) surface. The interaction between CH_4 and metal surfaces exhibits an evident weakness, suggesting physisorption. This observation aligns with previous studies on the physisorption of CH_4 on several metal surfaces, including Rh(111) [25], Pd (100) [26], etc.

3.2 CH₄ Dissociation on Metal Surface

In this section, the dissociative process of CH_4 into CH_3 + H was investigated at the coverage of 0.11 ML. The initial state, TS and final state structures are illustrated in Figure 2.
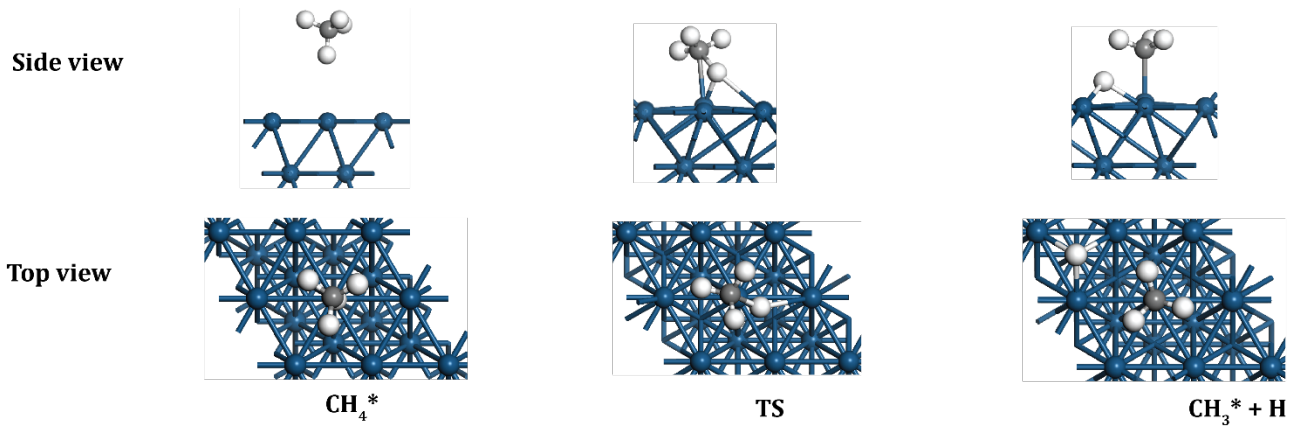
Fig. 2 *Reactant, TS and product structures for $CH_4 \rightarrow CH_3$ + H reaction on Ir(111) surface*
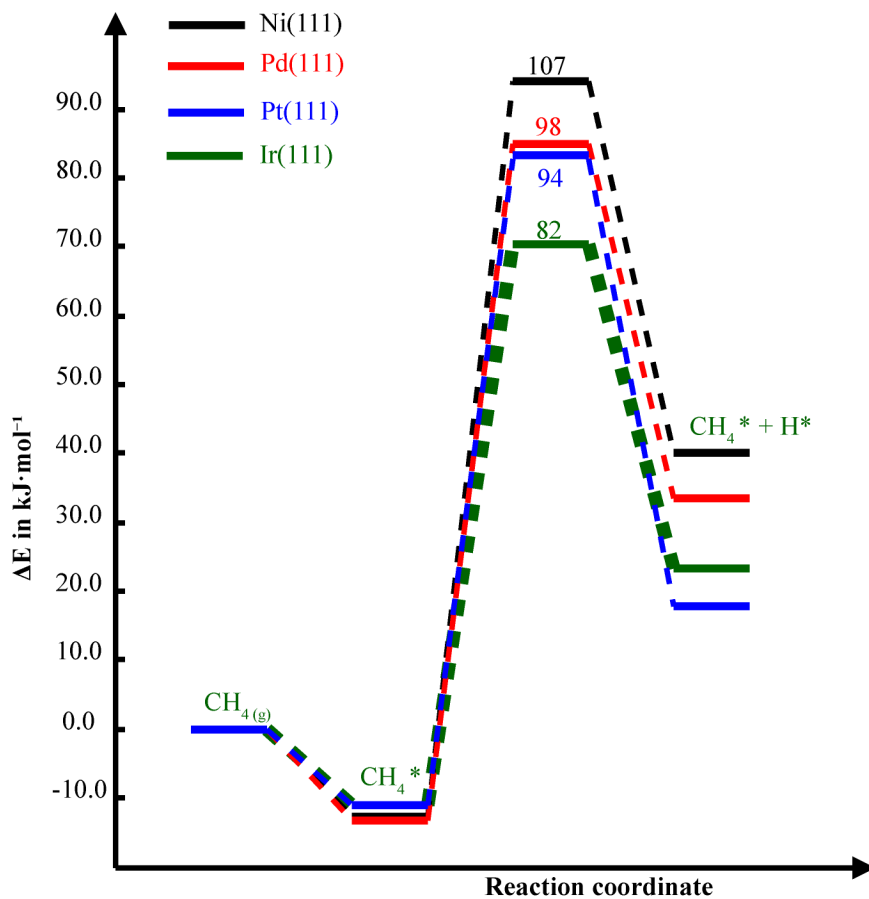
Fig. 3 *The energy profiles of CH_4 to CH_3 dissociation on metal (111) surfaces*

Based on the data depicted in Figure 3, it is evident that the initial stage entails the adsorption of CH_4 onto the surface. Subsequently, the adsorbed CH_4^* species undergoes dissociation, resulting in the formation of CH_3^* and H^* species. The relative activation energies for the surfaces of Ir(111), Ni(111), Pd(111), and Pt(111) are 92, 114, 127, and 116 kJ/mol. The activation barrier for the dissociation of CH_4 on the Ir(111) surface is consistent

with the values reported by Qiet et al [21], specifically 89.7 kJ/mol at a coverage of 0.25 ML. This finding is also in keeping with experimental results [27]which reported an activation barrier of 106 kJ/mol. Based on the calculation results, it can be concluded that methane dissociation has a higher preference for the Ir(111) surface than other metal surfaces.

3.3 Adsorption of H_2O on M(111) Surface at Different Coverage

The investigation focused on examining various orientations of water adsorption at the atop site. Table 2 presents a summary of the adsorption energies (E_{ads}), the height of water from the metal surface (h_{M-O}) and the bond length between oxygen atom and hydrogen atoms at 1.00, 0.50, 0.25, and 0.11 monolayer. The most favourable adsorption location for H_2O on the Ni(111) surface is the atop position, where the H_2O molecule is oriented parallel to the nickel surface. The adsorption energies of H_2O molecules on a nickel surface (Ni(111)) at different coverages, specifically 1.00, 0.50, 0.25, and 0.11 ML, are recorded as -5.22, -38.19, -42.23, and -44.76 kJ/mol, respectively. The findings align with the empirical evidence presented in a prior investigation., which determined the value to be -42.45 kJ/mol [9]. The distance between the Ni(111) surface and H_2O molecules drops from 3.27 to 2.44 Å when the coverage reduces from 1.00 to 0.11 ML due to the increased interaction between the H_2O molecule and the Ni(111) surface. The adsorption energies of water molecules on Ir(111), Ni(111), Pd(111), and Pt(111) surfaces, with a coverage of 0.11 monolayers (ML), are -58.04, -46.07, -45.81, and -44.76 kJ/mol, respectively. The water molecule exhibits the most pronounced interactions with the Ir(111) surface.

Table 2 *H_2O adsorption on metal (111) surface*

Metal Surface	Adsorption site	0.11 ML			0.25 ML		
		h_{M-O} (Å)	d_{O-H} (Å)	E_{ads} (kJ/mol)	h_{M-O} (Å)	d_{O-H} (Å)	E_{ads} (kJ/mol)
Pt(111)	atop	2.44	0.977	-45.81	2.53	0.977	-42.53
Pd(111)	atop	2.43	0.976	-45.76	2.53	0.977	-42.53
Ir(111)	atop	2.34	0.979	-58.04	2.38	0.981	-54.43
Ni(111)	atop	2.21	0.978	-44.76	2.29	0.979	-42.23

| Metal Surface	Adsorption site	0.50 ML			1.00 ML		
		h_{M-O} (Å)	d_{O-H} (Å)	E_{ads} (kJ/mol)	h_{M-O} (Å)	d_{O-H} (Å)	E_{ads} (kJ/mol)
Pt(111)	atop	2.76	0.985	-53.68	3.28	0.978	-46.07
Pd(111)	atop	2.66	0.985	-55.72	3.18	0.981	-46.55
Ir(111)	atop	2.57	0.987	-58.45	3.30	0.982	-43.00
Ni(111)	atop	2.73	1.007	-38.19	3.27	0.985	-5.22

3.4 Aggregation of H_2O on Metal Surface

The most stable water adsorption configurations were identified using a stepwise adsorption energy analysis [9]. The strength of hydrogen bond interaction within the $(H_2O)_n$ cluster is directly proportional to the magnitude of the negative hydrogen-bond interaction (E_H). The more negative Eads, the stronger the interaction of $(H_2O)_n$ cluster with the metal surface [8]. The most stable arrangements of H_2O clusters on the metal surfaces are shown in Figure 4. Table 3 displays the E_H, formation energy, and adsorption energy of the $(H_2O)_n$ cluster on metal surfaces. The findings of this study indicate that a rise in the quantity of aggregate water molecules leads to an increased hydrogen-bond interaction among these molecules. Consequently, the interaction between water and metal surfaces weakens, aligning with the findings of Hao et al. [8]. The interaction between water molecules was found to be strongest on the Ir (111) surface, while the Ni(111) surface exhibited the smallest interaction.

Table 3 *H_2O aggregation on metal (111) surface*

$(H_2O)_n$	Ir(111) surface			Pt(111) surface		
	E_{form} (kJ/mol)	E_H (kJ/mol)	E_{ads}^c (kJ/mol)	E_{form} (kJ/mol)	E_H (kJ/mol)	E_{ads}^c (kJ/mol)
1	-54.43	0.00	-54.43	-42.53	0.00	-42.53
2	-62.81	-13.71	-49.10	-55.71	-13.71	-42.00
3	-71.43	-29.83	-41.60	-66.23	-29.83	-36.40
4	-70.46	-37.40	-33.07	-64.75	-37.40	-27.35

$(H_2O)_n$	Pd(111) surface			Ni(111) surface		
	E_{form} (kJ/mol)	E_H (kJ/mol)	E_{ads}^c (kJ/mol)	E_{form} (kJ/mol)	E_H (kJ/mol)	E_{ads}^c (kJ/mol)
1	-43.72	0.00	-43.72	-42.16	0.00	-42.16
2	-56.54	-13.71	-42.83	-52.94	-13.71	-39.22
3	-65.05	-29.83	-35.22	-57.65	-29.83	-27.82
4	-69.17	-37.40	-31.77	-61.10	-37.40	-23.70
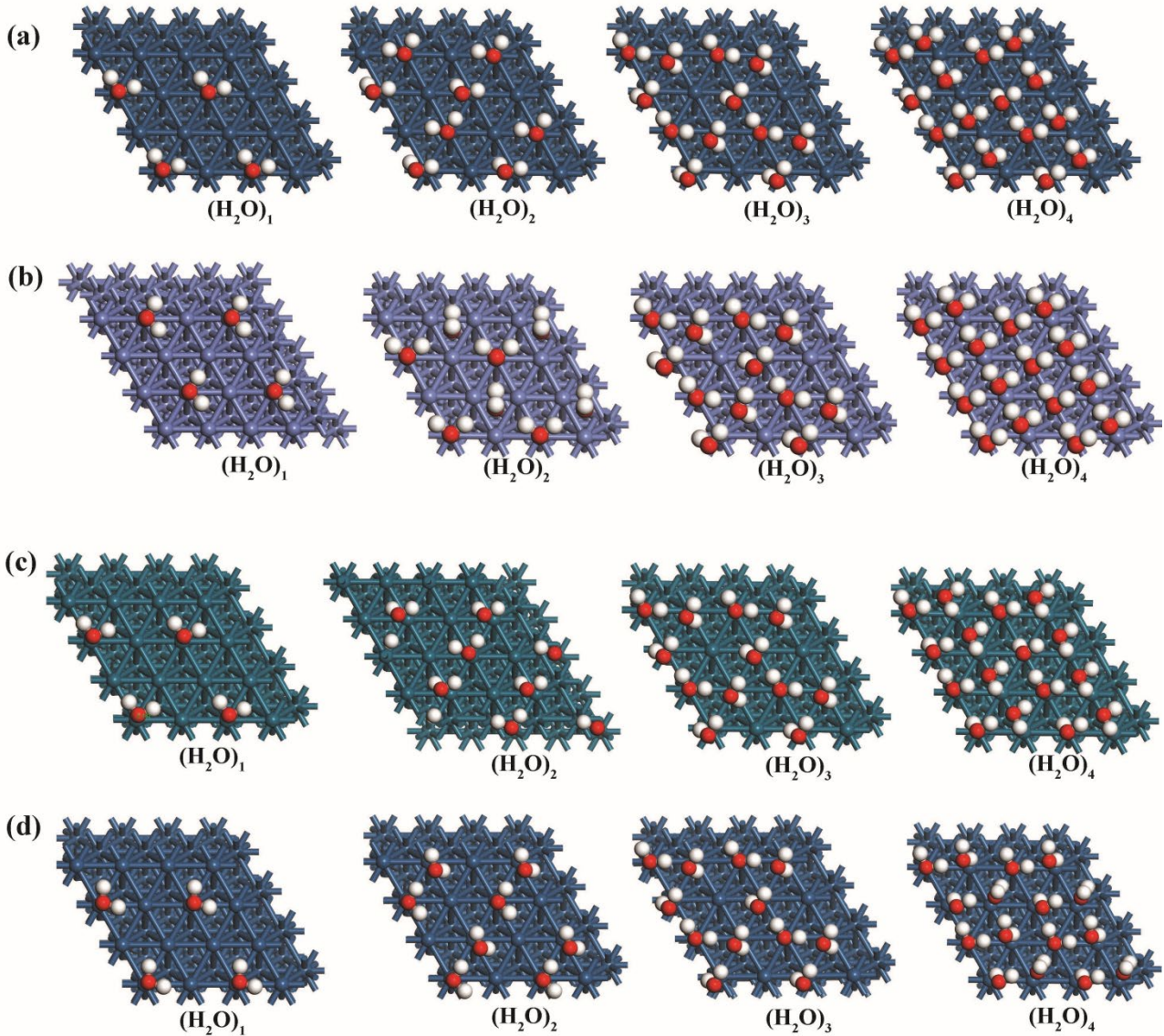
Fig. 4 *Adsorption of most stable water aggregation configurations on(a) Ir(111) (b) Ni(111) (c) Pd(111) (d) Pt(111) surfaces*

3.5 Thermodynamics

In accordance with equation 7, we employed the parameter Γ as a benchmark to evaluate the stability of the adsorbed system of H_2O and CH_4 under various conditions. It was observed that a greater negative value of Γ corresponded to a higher degree of stability in the adsorbed structure [28]. Figure 5 illustrates the relationship between the surface free Gibbs energy of the adsorbate, specifically H_2O and CH_4, and temperature at a pressure of 1 bar for each respective surface.
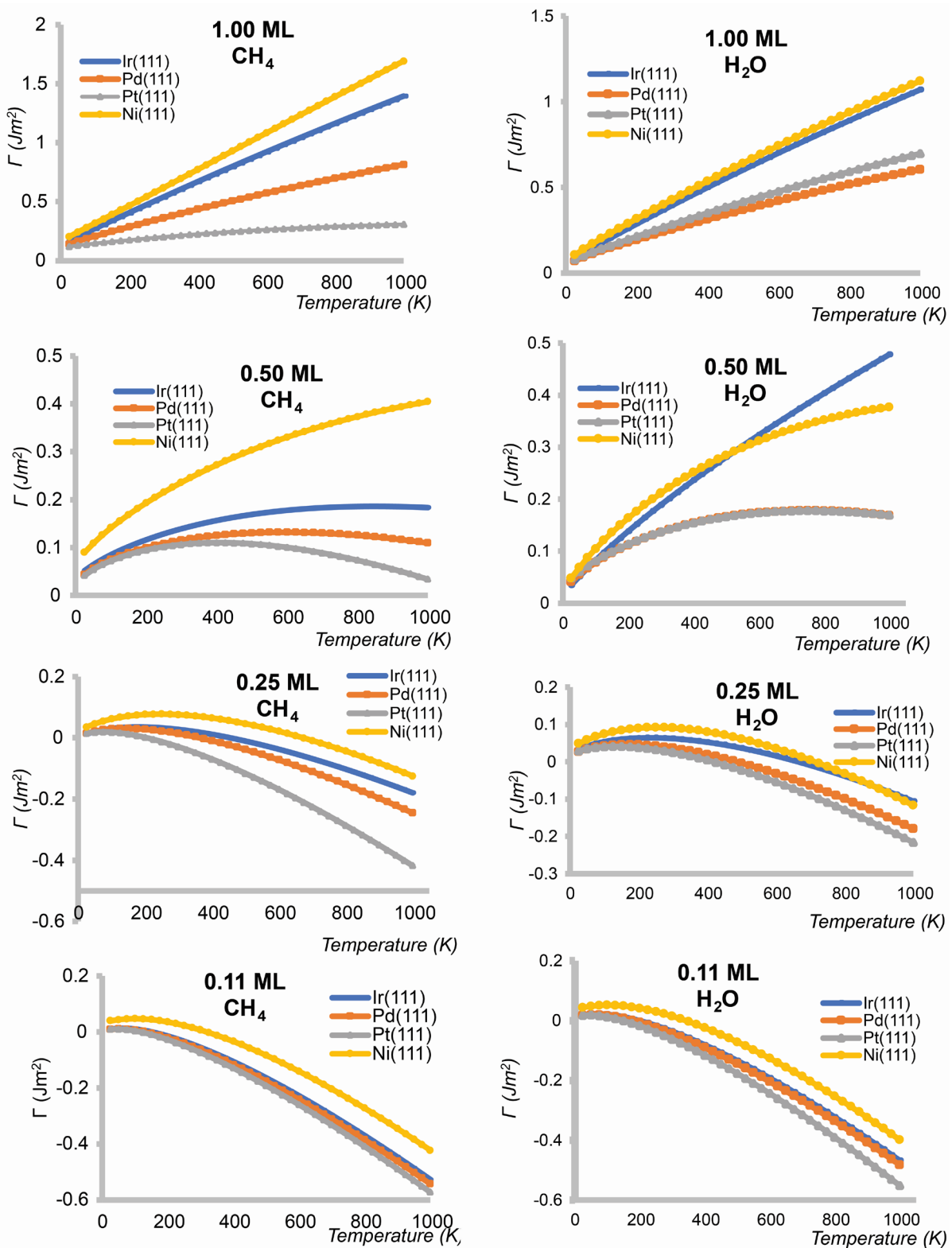
Fig. 5 *SGF energies as a function of temperature at 1 bar for H₂O and CH₄ adsorption on Ir(111), Ni(111), Pd(111) and Pt(111) surface*

The experimental findings indicated that the surface-free Gibbs energy associated with the adsorption of methane and water on the metal surface exhibited positive values when the coverage reached 0.50 and 1.00 monolayers (ML). The surface-free Gibbs energy exhibited a negative value at coverage levels of 0.25 and 0.11 ML on the metal surfaces. The thermodynamically most stable coverage for water and methane adsorption at all adsorbate coverages was found to be the Pt(111) surface. The order of stability for water and methane

adsorption on various surfaces, rated from highest to lowest, is as follows: Pt(1 1 1), Pd(1 1 1), Ir(1 1 1), and Ni(111).

4. Conclusion

This study explores the adsorption of CH_4 and H_2O on Pt(111), Ni(111), Ir(111), and Pd(111) surfaces at varying coverages and adsorption sites. Additionally, the aggregation of H_2O on these metal surfaces is examined through the utilisation of DFT calculations.

The preferred adsorption site for methane on the metal surface is located at the top position. The thermodynamic stability of methane adsorption on metal surfaces was determined to be unstable at coverage levels of 0.50 and 1.00 monolayers (ML), whereas it was found to be stable at coverage levels of 0.25 and 0.11 ML. The order of decreasing activation energies for the dissociation of CH_4 to CH_3 on various surfaces is as follows: Pd(111) > Pt(111) > Ni(111) > Ir(111).

In the context of H_2O adsorption on metal surfaces, a reduction in water coverage on the surface leads to a corresponding decrease in the height of the water layer above the metal surface. An increase in the adsorption energy accompanies this decrease in coverage. The number of H_2O molecules present influences the aggregation of H_2O on metal surfaces. An increase in the quantity of H_2O molecules leads to a greater interaction of hydrogen bonds among the water molecules. Consequently, this decreases the interaction between the H_2O molecules and the metal surfaces. The thermal stability of methane and water on different surfaces can be ranked in descending order as follows: Pt(111) > Pd(111) > Ir(111) > Ni(111).

Acknowledgement

Conflict of Interest

Authors declare that there is no conflict of interests regarding the publication of the paper.

References

[1]   Roy, G., & Chattopadhyay, A. P. (2017). Dissociation of methane on Ni_4 cluster-A DFT study. *Computational and Theoretical Chemistry*, *1106*, 7-14.

[2]   Wang, F., Li, Y., Wang, Y., Zhang, C., Chu, L., Yang, L., & Fan, X. (2022). Mechanism insights into sorption enhanced methane steam reforming using Ni-doped CaO for H2 production by DFT study. *Fuel*, *319*, 123849.

[3]   Khurana, D., Dahiya, N., Negi, S., Bordoloi, A., Ali Haider, M., Bal, R., & Khan, T. S. (2023). Improving the Coke Resistance of Ni-Ceria Catalysts for Partial Oxidation of Methane to Syngas: Experimental and Computational Study. *Chemistry – An Asian Journal*, *18*(7), e202201298.

[4]   Tang, L., Huang, X., Ran, J., Guo, F., Niu, J., Qiu, H., Ou, Z., Yan, Y., Yang, Z., Qin, C. (2022). Density functional theory studies on direct and oxygen assisted activation of C–H bond for dry reforming of methane over Rh–Ni catalyst. *International Journal of Hydrogen Energy*, 47(71), 30391-30403,

[5]   Che, F., Gray, J.T., Ha, S., McEwen, J.-S. (2017). Improving Ni Catalysts Using Electric Fields: A DFT and Experimental Study of the Methane Steam Reforming Reaction. *ACS Catalysis*, 7(1), 551-562.

[6]   Xu, Y., Lausche, A.C., Wang, S., Khan, T.S., Abild-Pedersen, F., Studt, F., Nørskov, J.K., Bligaard, T. (2013). In silico search for novel methane steam reforming catalysts. *New Journal of Physics*, 15(12), 125021.

[7]   Canduela-Rodriguez, G., Sabbe, M.K., Reyniers, M.-F., Joly, J.-F., Marin, G.B. (2014). Thermodynamic study of benzene and hydrogen coadsorption on Pd (111). *Physical Chemistry Chemical Physics*, 16(43), 23754-23768.

[8]   Hao, X., Zhang, R., He, L., Huang, Z., Wang, B. (2018). Coverage-dependent adsorption, dissociation and aggregation of H_2O on the clean and pre-adsorbed oxygen Cu (111) surface: A DFT study. *Molecular Catalysis*, 445, 152-162.

[9]   Zhu, L., Liu, C., Wen, X., Li, Y.-W., Jiao, H. (2019). Molecular or dissociative adsorption of water on clean and oxygen pre-covered Ni (111) surfaces. *Catalysis Science & Technology*, 9(1), 199-212, Article.

[10] Catapan, R.C., Oliveira, A.A., Chen, Y., Vlachos, D.G. (2012). DFT study of the water–gas shift reaction and coke formation on Ni (111) and Ni (211) surfaces. *The Journal of Physical Chemistry C*, 116(38), 20281-20291, Article.

[11] Pache, T., Steinrück, H.-P., Huber, W., Menzel, D. (1989). The adsorption of H_2O on clean and oxygen precovered Ni (111) studied by ARUPS and TPD. *Surface Science*, 224(1-3), 195-214, Article.

[12] Chen, L., Ueta, H., Chadwick, H., Beck, R.D. (2015). The Negligible Role of C–H Stretch Excitation in the Physisorption of CH_4 on Pt (111). *The Journal of Physical Chemistry C*, 119(26), 14499-14505, Article.

[13] Delley, B. (2000). From molecules to solids with the DMol 3 approach. *The Journal of chemical physics*, 113(18), 7756-7764, Article.
[14] Burke, K., Perdew, J. P., & Wang, Y. (1998). Derivation of a generalized gradient approximation: The PW91 density functional. In *Electronic Density Functional Theory: recent progress and new directions* (pp. 81-111). Springer.
[15] Bergner, A., Dolg, M., Küchle, W., Stoll, H., Preuß, H. (1993). Ab initio energy-adjusted pseudopotentials for elements of groups 13–17. *Molecular Physics*, 80(6), 1431-1441, Article.
[16] Ibach, H., Lüth, H. (2009). *Solid-state physics: an introduction to principles of materials science.* Springer Science & Business Media.
[17] Haas, P., Tran, F., Blaha, P. (2009). Calculation of the lattice constant of solids with semilocal functionals. Physical Review B, 79(8), Article.
[18] Kittel, C. (2005). *Introduction to solid state physics.* John Wiley & sons, inc.
[19] Grégoire Padró, C. E., & Keller, J. O. (2000). Hydrogen energy. *Kirk-Othmer Encyclopedia of Chemical Technology*.
[20] Yang, M.-L., Zhu, Y.-A., Fan, C., Sui, Z.-J., Chen, D., & Zhou, X.-G. (2010). Density functional study of the chemisorption of C_1, C_2 and C_3 intermediates in propane dissociation on Pt (1 1 1). *Journal of molecular catalysis A: Chemical*, *321*(1-2), 42-49.
[21] Qi, Q., Wang, X., Chen, L., & Li, B. (2013). Methane dissociation on Pt (1 1 1), Ir (1 1 1) and PtIr (1 1 1) surface: A density functional theory study. *Applied Surface Science*, *284*, 784-791.
[22] Gautier, S., Steinmann, S. N., Michel, C., Fleurat-Lessard, P., & Sautet, P. (2015). Molecular adsorption at Pt (111). How accurate are DFT functionals? *Physical Chemistry Chemical Physics*, *17*(43), 28921-28930.
[23] Jiang, Z., Li, L., Xu, J., & Fang, T. (2013). Density functional periodic study of the dehydrogenation of methane on Pd (1 1 1) surface. *Applied Surface Science*, *286*, 115-120.
[24] Kalantari Fotooh, F., & Nayeri, M. (2021). Methane adsorption on the surface of metal (Fe, Ni, Pd) decorated SWCNT: A density functional theory (DFT) study. *Surface Science*, *713*, 121913.
[25] Wang, B., Song, L., & Zhang, R. (2012). The dehydrogenation of CH4 on Rh (1 1 1), Rh (1 1 0) and Rh (1 0 0) surfaces: A density functional theory study. *Applied Surface Science*, *258*(8), 3714-3722.
[26] Zhang, C. J., & Hu, P. (2002). Methane transformation to carbon and hydrogen on Pd (100): Pathways and energetics from density functional theory calculations. *The Journal of Chemical Physics*, *116*(1), 322-327.
[27] Hamza, A., Steinruck, H. P., & Madix, R. (1987). The dynamics of the dissociative adsorption of alkanes on Ir (110). *The Journal of Chemical Physics*, *86*(11), 6506-6514.
[28] Zhao, P., He, Y., Cao, D.-B., Wen, X., Xiang, H., Li, Y.-W., Wang, J., & Jiao, H. (2015). High coverage adsorption and co-adsorption of CO and H_2 on Ru(0001) from DFT and thermodynamics. *Physical Chemistry Chemical Physics*, *17*(29), 19446-19456.